A subset of *Plasmodium falciparum* RIFINs is linked to severe malaria risk reduction and engages LILRB1 through a conserved structural motif

Kokouvi Kassegne,[a,b,*] Hai-Mo Shen,[a] Shen-Bo Chen,[a] Shao-Jie Xu,[a] Jinyu Li,[c] Bin Xu,[a] Kirk W. Deitsch,[d] Yue Wang,[e] Xiao-Nong Zhou,[a,b,f] and Jun-Hu Chen[a,b,e,f,**]

[a]National Key Laboratory of Intelligent Tracking and Forecasting for Infectious Diseases, National Institute of Parasitic Diseases, Chinese Center for Disease Control and Prevention (Chinese Center for Tropical Diseases Research), National Health Commission of the People's Republic of China (NHC) Key Laboratory of Parasite and Vector Biology, World Health Organization (WHO) Collaborating Center for Tropical Diseases, National Center for International Research on Tropical Diseases, Shanghai, 200025, P. R. China
[b]School of Global Health, Chinese Centre for Tropical Diseases Research, Shanghai Jiao Tong University School of Medicine, Shanghai, 200025, P. R. China
[c]College of Chemistry, Fuzhou University, Fuzhou, Fujian, 350108, P. R. China
[d]Department of Microbiology and Immunology, Weill Cornell Medicine, Cornell University, Ithaca, NY, 14853, USA
[e]School of Basic Medical Sciences and Forensic Medicine, Hangzhou Medical College, Hangzhou, 310013, P. R. China
[f]Hainan Tropical Diseases Research Center (Hainan Sub-Center, Chinese Center for Tropical Diseases Research), Haikou, 571199, P. R. China

eBioMedicine
2025;122: 106041
Published Online xxx
https://doi.org/10.1016/j.ebiom.2025.106041

Summary

Background RIFIN proteins are key mediators of *Plasmodium falciparum* immune evasion through antigenic variation and inhibitory receptor interactions; however, some RIFIN variants elicit protective antibody responses in individuals with malaria. While it is not surprising that RIFINs provoke immune responses, the functional and structural basis of both the association of RIFINs with clinical outcomes and their engagement with inhibitory receptors remains a critical knowledge gap in malaria immunology.

Methods In a systematic immunoproteomic analysis that uses protein microarrays, we profiled anti-RIFIN antibody responses in individuals with malaria and correlated these responses with disease severity. Candidate RIFINs linked to severe malaria risk reduction were identified and validated via logistic regression analyses. The functional and structural basis of these RIFIN candidates was assessed via surface plasmon resonance (SPR) binding assays and structural modelling, with mechanistic insights derived from crystallographic analyses of LILRB1–RIFIN complexes and synthetic peptide interaction studies.

Findings We identified a RIFIN subset associated with a reduced risk of severe malaria. These RIFINs engage the inhibitory receptor LILRB1 through a conserved structural motif anchored by disulfide-bonded cysteines, despite overwhelming sequence diversity across the RIFIN family. LILRB1 binds both RIFINs and MHC-I ligands by overlapping interfaces, confirming that a convergent recognition strategy is exploited by the malaria pathogens and their hosts.

Interpretation Our study identified a bifunctional RIFIN subset that balances clinical immunity and immune evasion through a structurally conserved LILRB1-binding motif. These findings provide a blueprint for rational intervention strategies: the motif can guide vaccine design to overcome diversity by (1) eliciting antibodies to the structurally constrained, functional site or (2) disrupting immune evasion while leaving other protective epitopes. This work improves our understanding of RIFIN biology and opens new avenues to disrupt *P. falciparum* severe pathogenesis and reduce the global malaria burden.

*Corresponding author. National Key Laboratory of Intelligent Tracking and Forecasting for Infectious Diseases, National Institute of Parasitic Diseases, Chinese Center for Disease Control and Prevention (Chinese Center for Tropical Diseases Research), National Health Commission of the People's Republic of China (NHC) Key Laboratory of Parasite and Vector Biology, World Health Organization (WHO) Collaborating Center for Tropical Diseases, National Center for International Research on Tropical Diseases, Shanghai, 200025, P. R. China.
**Corresponding author. National Key Laboratory of Intelligent Tracking and Forecasting for Infectious Diseases, National Institute of Parasitic Diseases, Chinese Center for Disease Control and Prevention (Chinese Center for Tropical Diseases Research), National Health Commission of the People's Republic of China (NHC) Key Laboratory of Parasite and Vector Biology, World Health Organization (WHO) Collaborating Center for Tropical Diseases, National Center for International Research on Tropical Diseases, Shanghai, 200025, P. R. China.
E-mail addresses: ephremk@hotmail.fr (K. Kassegne), chenjh@nipd.chinacdc.cn (J.-H. Chen), shenhm@nipd.chinacdc.cn (H.-M. Shen), chensb@nipd.chinacdc.cn (S.-B. Chen), Xushaojie0420@163.com (S.-J. Xu), j.li@fzu.edu.cn (J. Li), xubin@nipd.chinacdc.cn (B. Xu), kwd2001@med.cornell.edu (K.W. Deitsch), wangyuerr@hmc.edu.cn (Y. Wang), zhouxn1@chinacdc.cn (X.-N. Zhou).
Teaser: A subset of *P. falciparum* RIFINs implicated in reduced severe malaria risk engages the immune receptor LILRB1 via a conserved structural motif, revealing a dual role for these virulence proteins and identifying a new axis for malaria intervention.

Funding Shanghai Natural Science Foundation (Grant No. 24ZR1473200); Bill & Melinda Gates Foundation (Grant No. INV-003421); National Key Research and Development Program of China (Grant Nos. 2018YFE0121600 and 2016YFC1202000); Special Fund for Health Research in the Public Interest (Grant No. 201202019); National Natural Science Foundation of China (Grant No. 81702032); Open Grant of the NHC Key Laboratory of Parasite and Vector Biology (National Institute of Parasitic Diseases, Chinese Center for Diseases Control and Prevention; Grant No. NHCKFKT2021-04).

Keywords: *Plasmodium falciparum*; Severe malaria risk; Immune evasion; RIFIN; LILRB1; Structural conservation; Clinical immunity

Introduction

Malaria remains one of the most devastating infectious diseases worldwide, affecting more than 200 million people and causing approximately half a million deaths annually. *Plasmodium falciparum* (Pf), the deadliest malaria parasite, is responsible for the majority of these fatalities, predominantly among young African children.[1] A cornerstone of Pf virulence lies in its ability to sequentially express distinct variant surface antigens (VSAs) on infected erythrocytes (IEs) through clonal variation, enabling continuous host immune evasion and parasite survival. Among these, the repetitive interspersed families of polypeptides (RIFINs), encoded by approximately 150 *rif* genes per parasite genome, represent the largest and one of the most polymorphic families of Pf surface antigens, although their diversity is complemented by the extensive variation observed in other antigen families, such as Pf erythrocyte membrane protein 1 (PfEMP1) and subtelomeric variant open reading frames (STEVORs).[2–4]

Research in Context

Evidence before this study

Malaria remains a leading cause of global morbidity and mortality, driven primarily by the ability of *Plasmodium falciparum* to evade host immunity through variant surface antigens (VSAs). Among these, RIFINs represent the largest and one of the most polymorphic families and are implicated in both immune evasion and clinical immunity. Previous studies established that anti-RIFIN antibodies are associated with reduced parasite density and milder clinical outcomes in endemic populations. Structural work revealed that some RIFINs engage the inhibitory receptor LILRB1 by mimicking host MHC-I, facilitating immune suppression. However, these studies were limited by narrow antigen coverage, lack of clinical correlation, or absence of mechanistic links between antibody responses, receptor binding, and disease outcomes. The functional and structural basis underlying the role of RIFINs—in both promoting severe disease and eliciting immunity—remains unresolved, hindering translational progress.

Added value of this study

This study integrates high-throughput immunoproteomics, structural biology, and biophysical validation to bridge this critical knowledge gap. Using protein microarrays probed with well-stratified clinical samples from severe and nonsevere malaria cases, we identified a subset of RIFINs associated with a reduced risk of severe malaria. We demonstrated that these clinically relevant RIFINs function as high-to moderate-affinity ligands for LILRB1, despite extreme sequence diversity. Through structural modelling, molecular dynamics simulations, and mutagenesis, we confirmed a conserved disulfide-anchored structural motif that enables molecular mimicry of MHC-I and facilitates receptor engagement. This motif—centered on invariant cysteine pairs and key interfacial residues—represents a structural vulnerability conserved across diverse RIFIN variants. Our findings provide direct evidence linking specific RIFIN subtypes to both clinical immunity and immune evasion mechanisms, offering a unified model for their role in severe malaria pathogenesis.

Implications of all the available evidence

The convergence of the clinical, immunological, and structural data presented here redefines RIFINs as bifunctional antigens capable of balancing clinical immunity and immune evasion through a structurally conserved interface. These findings have profound implications for malaria intervention strategies. The identified motif provides a blueprint for rational vaccine design aimed at eliciting antibodies that could disrupt LILRB1 engagement across diverse RIFIN strains. It also opens avenues for developing monoclonal antibodies or small-molecule inhibitors that could target this conserved functional site. By demonstrating that naturally acquired antibodies to specific RIFIN variants correlate with milder malaria outcomes, our work supports their use as biomarkers for disease risk stratification and vaccine efficacy monitoring. Ultimately, these insights could accelerate the development of next-generation tools to combat severe malaria and reduce the global burden of this devastating disease.

RIFINs are classified into two major groups: A-type and B-type.[5] A-RIFINs, which constitute approximately 70% of the family, are distinguished by a 25-amino acid (aa) insertion at the N-terminus and are expressed on the IE surface and apical merozoites. In contrast, B-RIFINs lack this insertion and are primarily retained within parasitized erythrocytes.[6] Transcriptional analyses of clinical isolates revealed significantly higher expression levels of A-RIFINs than B-RIFINs, underscoring their critical role in parasite survival and pathogenesis within the human host.[7]

Functionally, RIFINs are implicated in malaria severity through multiple mechanisms demonstrated in experimental systems: they mediate IE sequestration by promoting rosetting (the binding of IEs to uninfected erythrocytes),[8] and they facilitate immune evasion by engaging inhibitory receptors on immune cells, including leukocyte immunoglobulin-like receptor B1 (LILRB1) and leukocyte-associated immunoglobulin-like receptor 1 (LAIR1).[9,10] Their role in natural infections is supported by seroepidemiological studies linking anti-RIFIN antibodies to clinical outcomes.[11]

Despite their role in immune evasion, RIFINs also elicit antibody responses that are correlated with clinical outcomes in individuals from malaria-endemic regions, which is consistent with the broader pattern observed for other variant antigen families, such as PfEMP1 and STEVORs.[12,13] Studies have demonstrated that anti-RIFIN antibodies constitute a major component of the humoral response against IEs. High titres of anti-RIFIN immunoglobulin G (IgG) antibodies correlate with rapid parasite clearance and the suppression of malaria symptoms in asymptomatic children.[11] Recent work has shown that human monoclonal antibodies can specifically recognize and immunoprecipitate IEs via RIFIN family members,[14] suggesting that these antigens may represent viable targets for protective immunity.

However, the development of RIFIN-based interventions faces significant challenges because of the extreme diversity and clonal variation of antigens.[2,3] Parasites evade host immunity by sequentially expressing different RIFIN variants, leading to recurrent infections. The host gradually develops a broad antibody repertoire against multiple RIFINs over time, but some parasites escape through the expression of novel variants not yet recognized by existing antibodies. Some parasites survive within the host due to sequential expression of RIFINs, which are not yet targeted by the existing repertoire of host antibodies. This evolutionary and structural ingenuity position RIFINs as both foes and potential allies for severe malaria control. However, gaps persist: prior studies either focused on limited RIFIN subsets or were limited in identifying specific subtypes of anti-RIFIN antibodies that correlate with milder clinical outcomes of malaria,[11,15–17] leaving their translational potential unresolved. While the structural basis of RIFIN–LILRB1 binding has been elegantly revealed through crystallography,[10,18] the relationship between these interactions and clinical outcomes in natural infections remains poorly defined. Understanding which RIFIN variants engage LILRB1 in clinically relevant contexts is essential for rational vaccine design.

Natural immunity to severe malaria develops after repeated infections, with anti-RIFIN IgG playing a key role in reducing the risk of severe malaria or blocking IE adhesion.[8,11] This observation suggests that a vaccine mimicking natural immunity could prevent severe disease. However, such a vaccine would need to induce antibodies capable of recognizing diverse RIFIN variants while targeting conserved functional domains. Addressing this challenge requires the identification of RIFIN targets linked to improved clinical outcomes and detailed structural and biophysical insights into their interactions with receptors.

The central goal of this study was to resolve a fundamental question in Pf biology: how can the same family of VSAs—RIFINs—simultaneously drive immune evasion and elicit antibodies associated with a reduced risk of severe malaria? While it is not surprising that surface-exposed antigens provoke immune responses, the structural and functional basis enabling certain RIFINs to be associated with clinical outcomes has remained unclear.

In this study, we aimed to identify RIFIN variants associated with reduced severe malaria risk and characterize their interaction with the LILRB1-targeting mechanism for actionable targets of severe malaria intervention. We combined immunoproteomics, structural biology, immunogenomics, and biophysical approaches to systematically profile humoral responses to all A-RIFINs in severe and nonsevere malaria cases, identify RIFIN immunogens associated with uncomplicated malaria, and characterize their interaction with LILRB1.

Methods

Study design

We conducted a translational immunogen–ligand identification study integrating high-throughput immunoproteomics, structural biology, and biophysical validation to redefine RIFINs as actionable targets for malaria intervention. First, we systematically profiled humoral responses to all A-RIFINs using eukaryotic wheat germ cell-free (WGCF) protein microarrays[19,20] probed with sera from Togolese and Chinese cohorts (severe malaria [SMG; n = 112], uncomplicated malaria [NMG; n = 87], and uninfected controls [NCG; n = 67]).[21–23] Antibody signal intensity ratios and logistic regression analyses[24–26] allowed the identification of RIFIN responses linked to a reduced risk of severe malaria. Next, SPR assays confirmed these RIFINs as functional ligands for the immune inhibitor receptor LILRB1.[9] To resolve the

structural basis of this interaction, we modelled LILRB1 complexes with RIFINs and the physiological ligand β2M of MHC-I, revealing convergent binding interfaces despite the diversity of the RIFIN sequence. Finally, sequence logo and entropy analyses of the Pf 3D7 RIFIN sequences (n = 158) and SPR validation of synthetic wild-type/mutant peptides pinpointed the conserved disulfide-anchored motif critical for LILRB1 engagement—a vulnerability exploitable for rational intervention.

Study population and malaria context

Both the SMG and NMG malaria groups were from malaria-endemic areas in the southern regions of Togo—specifically, Lomé (Golfe Prefecture, Maritime Region; 6°12′56″N, 1°22′54″E), Atakpamé (Ogou Prefecture, Plateaux Region; 7°52′87″N, 1°13′05″E), and Agou-Gadzépé (Agou Prefecture, Plateaux Region; 7°28′01″N, 1°55′01″E). Lomé, the coastal capital of Togo, sits along the Gulf of Guinea and has an urban population of ~837,437 (2010 census). Despite its equatorial proximity, the city experiences a tropical savanna climate: a pronounced dry season (November–March) and bimodal rainy seasons (April–October), peaking in June and September. Annual rainfall averages 800–900 mm, with mean temperatures exceeding 27.5 °C—conditions that sustain year-round malaria transmission, albeit moderated by urbanization. In contrast, Agou (80 km north) and Atakpamé (161 km north) are rural and semi-rural, respectively, with populations of ~11,000 and 84,979 (2006 census), respectively. The tropical climate in the Plateaux Region features heavier rainfall—up to 2000 mm annually in Agou and 1300–1400 mm in Atakpamé—with average temperatures ranging from 23.5 to 26 °C.

These environmental differences shape distinct malaria dynamics: *Anopheles gambiae* drives perennial transmission, with intense rural transmission on Plateaux due to rice fields and stagnant water (*P. falciparum* > 90% prevalence), whereas the urban setting of Lomé has lower but sustained transmission, compounded by imported cases. Children under five years of age and pregnant women remain the most vulnerable, with higher burdens in agrarian communities of Plateaux than in urban centers of Maritime.

Samples were collected from subjects with malaria at the time of their initial presentation to health centres. All cases were first diagnosed via microscopic examination and subsequently confirmed via polymerase chain reaction (PCR).[22,23]

Selection of RIFIN targets

To identify clinically relevant A-RIFIN candidates, we implemented a stringent selection pipeline combining functional genomics and translational criteria. From the Pf 3D7 genome (PlasmoDB v.26: https://plasmodb.org), we selected 97 full-length A-RIFIN open reading frames (ORFs; 855–1146 bp) on the basis of (1) pathogenic relevance (association with antigenic variation, immune evasion, or erythrocyte aggregation), (2) structural integrity (transmembrane domains, surface localization signals), and (3) clinical prioritization (proteogenomic evidence linking expression to disease severity). Truncated or divergent sequences lacking homology to canonical RIFINs were excluded,[5,27] ensuring a focus on functional targets with intervention potential (Table S1).

While previous microarray studies have expressed larger numbers of RIFINs,[17] our library was specifically optimized to include A-RIFINs (61.39%) with strong pathogenic and clinical relevance, enabling a focused investigation into the mechanisms of immune evasion and clinical outcomes.

High-efficiency cloning of functionally relevant RIFIN antigen genes

To enable functional characterization of A-RIFINs, we optimized a high-fidelity cloning pipeline combining precision primer design and proofreading-enhanced amplification. Gene-specific primers with 5′ extensions (5′-GGG CGG ATA TCT CGA G-3′ and 5′-GCG GTA CCC GGG AATC CTT A-3′) were designed for infusion cloning (Table S2), ensuring seamless insertion into the linearized pEU-E01-His-N2 vector (CellFree Sciences).[28] ORFs were amplified from *P. falciparum* 3D7 cDNA via PrimeSTAR GXL DNA Polymerase (Takara), which was selected for its proofreading ability to minimize PCR errors, followed by high-efficiency recombination via an In-Fusion Advantage PCR Cloning Kit (CellFree Sciences) in a C1000 Touch Thermal Cycler (Bio-Rad) (Tables S3, S4). The transformed *Escherichia coli* DH5α-recombinant plasmid clones were selected via ampicillin resistance (100 μg/mL) on Luria Bertani agar plates and validated through PCR screening with recombination-specific primers (5′-CCA CTA ACC TAT CTA CAT-3′ and 5′-GGA AGG CCG GAT AAG ACG-3′), with final sequence confirmation performed by BGI Shanghai.

High-fidelity production of RIFIN and control proteins

To generate biologically active RIFINs for immunological studies, we employed an optimized eukaryotic WGCF expression platform.[20,29] Recombinant plasmids encoding A-RIFIN ORFs were purified via QIAGEN Plasmid Kits (Qiagen) and subjected to precisely controlled coupled transcription/translation (37 °C for 6 h and 15 °C for 20 h) via the WEPRO7240H system (CellFree Sciences) (Table S5). The expressed proteins were subjected to rigorous quality control: (1) centrifugation (12,000×*g*, 10 min) to isolate soluble fractions, followed by (2) Western blot verification via sodium dodecyl sulfate–polyacrylamide gel electrophoresis (SDS–PAGE), PVDF membrane (Millipore) transfer, and blocking (4 °C overnight) with 5% (m/v) bovine serum albumin (BSA: Sigma) in Tris-buffered saline

(TBS: Sangon). For detection, the blots were probed with anti-His antibodies: Penta·His antibody, BSA-free (Qiagen Cat# 34660, RRID: AB_2619735) at 1:1000 in TBS and HRP-conjugated goat anti-mouse IgG secondary (Sigma–Aldrich Cat# 12–349, RRID: AB_390192) at 1:5000 in TBS supplemented with 0.1% (v/v) Tween-20 (TBS-T: Sangon). Bound antibodies were visualized using diaminobenzidine (Thermo Fisher Scientific), creating a comprehensive library of recombinant RIFINs.

Morover, Pf antigens among potential malaria vaccine candidates, owing to their roles in erythrocyte invasion and immune recognition/immunogenicity, were also WGCF-expressed as non-VSA antigen controls.[20,30,31] These include: the Pf 42-kDa fragment of merozoite surface protein 1 ($MSP1_{-42}$; residues 1327–-1720; PlamoDB: PF3D7_0930300), apical membrane protein 1 (AMA1; residues 26–622; PlasmoDB: PF3D7_1133400), and apical merozoite protein (Pf34; residues 26–325; PlasmoDB: PF3D7_0419700).

Clinical cohort stratification

To validate our serological comparisons and delineate RIFIN-specific immune correlates, we analysed sera from three prospectively characterized cohorts.[22,23] These include the following: (1) severe malaria group (SMG, n = 112): rigorously classified per the WHO criteria,[32] requiring both: high parasite density (> 100,000/μL) and ≥ 1 clinical severity marker observed at presentation (which in our cohort was prostration, jaundice, repetitive vomiting, inability to tolerate oral therapy, and/or dark urine); (2) nonsevere malaria group (NMG, n = 87): Pf malaria symptomatic cases with uncomplicated parasitaemia; and (3) normal control group (NCG, n = 67). Sex data for all participants were self-reported during the initial clinical assessment. While it was recorded as a demographic variable, biological sex was not a primary factor in the study design or stratification of the SMG and NMG cohorts. The analytical focus of this immunoproteomic study was the correlation between anti-RIFIN antibody response and clinical disease severity.

The NCG cohort comprised two carefully stratified populations: Chinese controls (malaria-naive; PCR-negative individuals from nonendemic region (Hangzhou, China) with no history of malaria exposure) with baseline immunogenicity thresholds and Togolese controls (PCR-confirmed negative with ≥ 6 weeks since last potential exposure) accounting for background exposure.[18,19] This dual design ensured rigorous discrimination between naive and likely exposure-related antibody responses while controlling for residual immunity in endemic populations, therefore strengthening specificity.

Ethics compliance

This study adhered strictly to the Declaration of Helsinki principles. All human serum samples were obtained under written informed consent with dual ethical approval from the Ethics Committee of the National Institute of Parasitic Diseases (NIPD) at the Chinese Centre for Disease Control and Prevention (Reference numbers: 20160627, 20181203) and the Togo Ministry of Health's Bioethics Committee (Authorization N◦019/2019/MSHP/CBRS).[21,22] The samples were anonymized and processed following international biosafety guidelines (WHO/CDS/CSR/LYO/2004.11).

High-throughput RIFIN screening via protein microarrays

We performed comprehensive RIFIN antibody profiling via an optimized microarray platform.[20,21] Crude recombinant RIFIN proteins (n = 97) were mixed 1:1 with protein-spotting buffer (CapitalBio) in 384-well plates (Thermo Fisher Scientific) and spotted in duplicate onto nitrocellulose slides via a 48 Smart Arrayer (CapitalBio), alongside controls ($MSP1_{-42}$ antigen control and wheat germ lysate negative control). After overnight immobilization (4 °C), the chips were blocked (37 °C, 2 h) with 3% BSA (Sigma) in phosphate-buffered saline supplemented with 0.1% (v/v) Tween-20 (PBS-T: Sangon) and probed with 1:10 wheat germ lysate-preabsorbed human sera at a 1:200 dilution in 1% (m/v) BSA/PBS-T (37 °C, 1 h). Following PBS-T washes, bound IgG was detected with Alexa Fluor 546-conjugated anti-human IgG (Thermo Fisher Scientific Cat# A-21089, RRID: AB_2535745; 10 ng/μL), scanned with LuxScan HT24 (CapitablBio), and quantified via the fixed circle method in Microarray Image Analysis SpotData-Ver2.0 (CapitablBio). Signal intensity (SI) ratios were calculated relative to those of normal controls (NCG mean + 2SD cut-off), with hierarchical clustering (MeV 4.9) revealing distinct response patterns across the SMG, NMG, and NCG cohorts.

Purification and seroprofiling of antigen controls

Crude AMA1 and Pf34 control antigens obtained from WGCF protein expression were subjected to guanidine hydrochloride denaturation (2 volumes of 3 M) and stepwise refolding in pH 8.0 buffer (24 h, 4 °C), followed by dialysis (buffer: NaCl-150 mM, Tris–HCl-20 mM, glycerol 20%, 48 h), centrifugation (13,000 rpm, 4 °C, 20 min) and PEG20000 (Beyotime) concentration. The final purification was performed via Ni-NTA affinity chromatography (Qiagen). Purity and molecular weight were verified by reducing SDS−PAGE and Coomassie blue staining (Beyotime).

To evaluate the anti-AMA1 and anti-Pf34 IgG responses, 96-well plates (Thermo Fisher Scientific) were coated overnight at 4 °C with 100 μl/well of a 2 μg/ml protein mixture (1:100 dilution of 200 μg/ml stock in coating buffer; Sangon). After washing with PBST, the plates were blocked with 200 μl/well of ELISA diluent (Invitrogen) for 2 h at RT. Serum samples (n = 20 per

SMG/NMG group; 1:500 dilution) or negative controls (ELISA diluent alone) were added (100 µl/well) and incubated for 2 h at room temperature. After washing, bound IgG was detected via incubation with an HRP-conjugated goat anti-human Fc antibody (Abcam Cat# ab97225, RRID: AB_10680850) at a ratio of 1:10,000; for 1 h, followed by incubation with TMB substrate (Sigma–Aldrich; 10 min). The reactions were stopped with 100 µl/well stopping solution (Sigma–Aldrich), and the absorbance was measured at 450 nm (BioTek Synergy HTX). Control sera from the NCG cohort (China/Togo) were included for baseline comparison.

Recombinant production of the top immunoreactive RIFIN proteins

To optimize high-yield production, the five most immunoreactive RIFINs (PF3D7_0425900, PF3D7_0732400, PF3D7_0833100, PF3D7_0833400, PF3D7_0900200) and a LILRB1-binding positive control (PF3D7_1254800)[9,10] were C-terminally 6 × His-tagged and expressed in *E. coli* BL21 via the pET-32a and pET-SUMO vectors (GeneCreate Biological Engineering). Cultures of recombinant colonies in LB medium supplemented with kanamycin (50 µg/ml) were induced with 0.1 mM isopropyl β-D-1-thiogalactopyranoside (IPTG: TransGen) at an OD600 of 0.6 (8 h, 30 °C/18 °C). The cells were lysed via ultrasonication (200 W, 3 s on/off, 10 min) in PBS with 1 mM and 5 mM DL-dithiothreitol (Thermo Fisher Scientific), followed by centrifugation (10,000 rpm, 10 min, 4 °C). The solubilized proteins were subjected to purification as described above and yielded > 90% pure protein.

Quantitative analysis of RIFIN–LILRB1 interactions via surface plasmon resonance

We characterized RIFIN–LILRB1 binding kinetics via a BIAcore T200 system (GE Healthcare). Recombinant human LILRB1-ECD (Sino Biological) was immobilized on a CM5 chip (GE Healthcare) at 669.2 RU via amine coupling (GE Life Sciences) and probed with serial dilutions of purified RIFIN targets (100, 50, 25, 12.5, 6.25, 3.125 and 1.5625 nM in HBS-EP, pH 7.4, 25 °C) at 30 µl/min (120 s, association/300 s dissociation). Specific binding was calculated via blank surface subtraction, with kinetic parameters (KD) derived from global 1:1 fitting (BIAevaluation 1.0: GE Healthcare). To map critical interaction motifs, we designed synthetic peptides encompassing (1) the core binding site (residues 243–267) of PF3D7_0900200 (RIFIN-56_WT) and its F264A mutant (RIFIN-56_F264A) and (2) the LILRB1-binding region (residues 216–240) of PF3D7_1254800 (positive control).[9] All experiments used independently prepared protein replicates to ensure robustness.

Structural modelling of LILRB1–RIFIN interactions

To elucidate the structural basis of immune evasion, we integrated multiscale computational approaches to predict and refine the interaction interfaces between LILRB1 and RIFIN PF3D7_0900200. The variable domain (residues 169–321) of RIFIN PF3D7_0900200—was modelled via ColabFold[33] (integrating MMseqs2 homology search[34] with AlphaFold2/RoseTTAFold),[35,36] whereas the LILRB1 structure was extracted from its cocrystal with PF3D7_1254800 (PDB: 6ZDX).[10] Blind docking via ClusPro[37] identified two dominant binding modes, from which we selected the lowest-energy models (Model1 and Model2) representing distinct interaction interfaces.

Comparative interface analysis of LILRB1 complexes

To investigate the interaction motif features of immune-evading RIFINs and endogenous HLA ligands at the binding groove of LILRB1 for functional analyses, we performed rigorous structural comparisons of LILRB1 binding interfaces in both physiological (HLA-A*1101, PDB: 1P7Q) and pathogenic (RIFIN PF3D7_1254800, PDB: 6ZDX) complexes via interfaceResidues.py. Interface residues were defined by solvent-accessible surface area changes (> 0.75 $Å^2$ upon complexation). Our analysis included both predicted RIFIN binding modes (Model1 and Model2) from docking studies, with all structural visualizations generated in PyMOL v2.5 (Schrödinger, LLC).

Molecular dynamics (MD) simulations of the LILRB1–RIFIN complexes

To assess key molecules that are involved in stabilizing interactions between the binding groove of LILRB1 and the conserved core of the RIFINs that we prioritized, we further investigated the atomic-level insights into the mechanisms of immune evasion they facilitate. To this end, we performed 500-ns all-atom MD simulations (AMBER16, LINCS algorithm)[38,39] of both predicted LILRB1–RIFIN binding modes (Model1 and Model2) to assess complex stability. The systems were solvated in 0.15 M NaCl TIP3P water boxes (125 $Å^3$)[40,41] with protonation states assigned by H++ server predictions.[42] Using the AMBER-ff14SB force field,[43] we (1) minimized energy (5000 steps steepest descent and 5000 steps conjugate gradient), (2) gradually heated (0–300 K in 20 steps of 0.2 ns), and (3) maintained NPT conditions (Nosé–Hoover thermostat and Berendsen barostat).[44,45] Electrostatics were calculated via particle mesh-Ewald (PME)[46] with a 10 Å cut-off. From the last 100-ns trajectories, we identified representative conformations (1.0 Å RMSD clustering) and quantified hydrogen bonds (< 3.5 Å distance and < 30° angle between acceptor and donor atoms).

Quantitative binding free energy analysis

To precisely evaluate the interaction strengths between LILRB1 and RIFIN in different models, we calculated binding free energies (ΔG_{bind}) via the MM/GBSA approach on 1000 snapshots from the last 100 ns of the MD trajectories.[47–49] The MM/GBSA method has been

widely validated for identifying binding energy hotspots and guiding therapeutic design in protein–protein interaction systems. This method provides an optimal balance between accuracy and computational efficiency for protein–protein systems, outperforming both docking scores and MM/PBSA for nonmetalloprotein complexes. The energy terms were computed as:

$$\Delta G_{bind} \approx E_{gas} + \Delta G_{sol} = (E_{ele} + E_{vdW}) + \Delta G_{GB} + \Delta G_{SA}$$

where polar solvation (ΔG_{GB}) was calculated via the generalized Born approximation and nonpolar contributions ($\Delta G_{SA} = \gamma(SASA) + \beta$) via empirical constants (γ = 0.00542 kcal mol^{-1} Å^{-2}, β = 0.92 kcal mol^{-1}).[50] We omitted conformational entropy due to its computational uncertainty and system similarity.[49] This rigorous thermodynamic profiling, performed via the well-established MM/GBSA approach,[49,50] could be used to identify key energetic drivers of RIFIN Model1/Model2–LILRB1 binding and identify hotspots for potential therapeutic disruption.

Comprehensive sequence analysis of the LILRB1-binding domain of RIFIN variants

To identify key residues under evolutionary constraints that may be targeted for intervention strategies, we analysed 158 RIFIN sequences from the *P. falciparum* 3D7 genome (PlasmoDB v.26),[27] excluding pseudogenes and truncated variants.[5] Sequences were aligned via MUSCLE 3.8 (https://ebi.ac.uk/jdispatcher/msa/muscle) with default parameters,[51] followed by entropy calculation (Shannon Entropy-One (https://www.hiv.lanl.gov/content/sequence/ENTROPY/entropy.html):) to quantify variability across positions. Sequence logos were generated via WebLogo (http://weblogo.threeplusone.com)[52] to reveal conserved motifs within the LILRB1-binding interface and highlight structural elements.

Comprehensive statistical analysis of clinical correlations

To evaluate RIFIN immunoreactivity patterns across clinical phenotypes, all the statistical analyses were performed via GraphPad Prism v7.0, R v4.1 (R Foundation), and Microsoft Excel (Microsoft). Continuous variables (parasite density and antibody levels) were analysed via nonparametric tests (Mann–Whitney U test for two-group comparisons; Kruskal–Wallis test with Dunn's post hoc test for multiple groups), and the results are presented as medians (IQRs25–75) and whiskers (10th–90th percentiles). Categorical variables (sex ratios, immunoreactivity proportions) were assessed via Fisher's exact tests. Logistic regression models were used to evaluate the associations between disease severity (SMG vs NMG) and seroprevalence/age, generating receiver operating characteristic (ROC) curves and odds ratios with 95% CIs. All tests were two-tailed, with $P < 0.05$ considered statistically significant.

Role of funders

The funders were not involved in the study design, data collection, analysis, interpretation, or writing of report.

Results

Broad anti-RIFIN antibody responses correlate with a reduced risk of severe malaria

We systematically characterized humoral responses to all 97 A-RIFINs via a well-established high-throughput antigen screening pipeline combining in-fusion cloning, WGCF expression, and protein microarrays (Fig. S1).[19–21] Sequencing confirmed perfect alignment with the Pf 3D7 reference ORFs, with successful His6-tagged protein expression validated by Western blotting (Fig. S2). Microarrays were probed with sera from (1) SMG cases (n = 97), (2) NMG cases (n = 112) (Table 1), and (3) NCG cases (n = 67); (age range: 29 [22–47] years), including the 6-week exposure-free window for Togolese controls, a timeframe that aligns with anti-RIFIN antibody kinetics from prior longitudinal studies.[11] This stratified design enabled correlation analysis of RIFIN immunogenicity with a reduced risk of disease severity. Moreover, anti-RIFIN responses showed consistent patterns—no evidence of differential RIFIN immunogenicity—across

	Severe malaria group (SMG, n = 87)	Nonsevere malaria group (NMG, n = 112)	*P* value
Age groups, n			
Children (0–14 y.o.)	n = 79	n = 70	
C1 (0–5 y.o.)	34	27	
C2 (6–10 y.o.)	33	29	
C3 (11–14 y.o.)	12	14	
Adults (> 14 y.o.)	8	42	
Sex ratio (M/F)	1.45 (48/33)	0.52 (44/68)	0.2211[a]
Age, years Mean ± SD	7.2 ± 5.8	18.5 ± 18.2	**0.0026**[b]
Parasite density/µL Median (IQR25–75)	216,419 (107,427–480,000)	24,035 (2826–81,000)	**0.0286**[c]
Subphenotype[d], n (% of SMG)	Prostration, 59 (68%) Jaundice, 47 (54%) Repetitive vomiting, 43 (49%) Inability to tolerate oral therapy, 37 (43%) Dark urine, 32 (37%)	Fever, cold, shivering, or body aches.	
Symptom complexity	Only 1 symptom, 31 (36%) ≥ 2 symptoms, 56 (64%)		

Study participants were recruited from three malaria-endemic regions of southern Togo, which represent distinct transmission ecologies: (1) Lomé (urban, Golfe Prefecture; tropical savanna climate, annual rainfall 800–900 mm), (2) Agou-Gadzépé (rural, Plateaux Region; hyperendemic, 2000 mm rainfall), and (3) Atakpamé (semi-rural, Ogou Prefecture; 1300–1400 mm rainfall). All samples were collected at clinical presentation (pretreatment) and confirmed by microscopy and PCR. Subheadings are bolded for emphasis; within the data, a bold *P* value denotes statistical significance. y.o., years old; C1, children 0–5 years; C2, children 6–10 years; C3, children 11–14 years; A, adults > 14 years. [a]*P* value (two-sided $\chi 2$ test) indicates no evidence of sex difference between the NMG and SMG groups. [b]*P* value (two-tailed Student unpaired *t* test) indicates a significant difference across ages between the NMG and SMG groups. [c]*P* value (two-tailed Mann–Whitney U test) indicates a significant difference in parasite load between the NMG and SMG groups. [d]Severe malaria subphenotypes aligned with the WHO criteria.[32]

Table 1: **Parasitic clinical characteristics and biodata of subjects with malaria, whose serum samples were used to probe the RIFIN arrays.**

severe phenotypes (heterogenicity test, $P = 0.32$), strengthening our SMG grouping strategy.

Comparative analysis of serum immunoreactivity revealed differences across the clinical groups: while the control samples (NCG) were largely nonreactive, both the SMG and NMG groups exhibited comprehensive responses against multiple RIFINs (Fig. 1A, Fig. S3). Notably, NMG subjects demonstrated significantly stronger anti-RIFIN IgG levels than did SMG cases (Wilcoxon test, $P < 0.001$; Fig. 1B and C), with 31 RIFIN variants showing particularly discriminatory immunoreactivity (Fisher's exact test (two-sided) range $P = 0.0001$–0.045; Table S6). These IgG antibody signatures likely remained consistent across age groups (Kruskal–Wallis, $P < 0.0001$), suggesting the broad relevance of RIFIN-targeting immunity in severe malaria risk reduction.

Our logistic regression analysis revealed that both higher anti-RIFIN antibody levels ($\beta = -0.196$, $P < 0.001$) and increasing age ($\beta = -0.071$, $P < 0.001$) were independently associated with a reduced risk of severe malaria (model fit: Hosmer–Lemeshow, χ^2 test $P = 0.4625$). The predictive value of this association was aligned with the ROC analysis (AUC = 0.811). On average, each additional seropositive RIFIN was associated with a 17.8% reduction in severe disease odds (OR = 0.822), although effect sizes varied across specific RIFINs. Each year of age was associated with a 6.9% risk reduction (OR = 0.931) (Fig. 1D). These findings suggest that broader anti-RIFIN seropositivity—

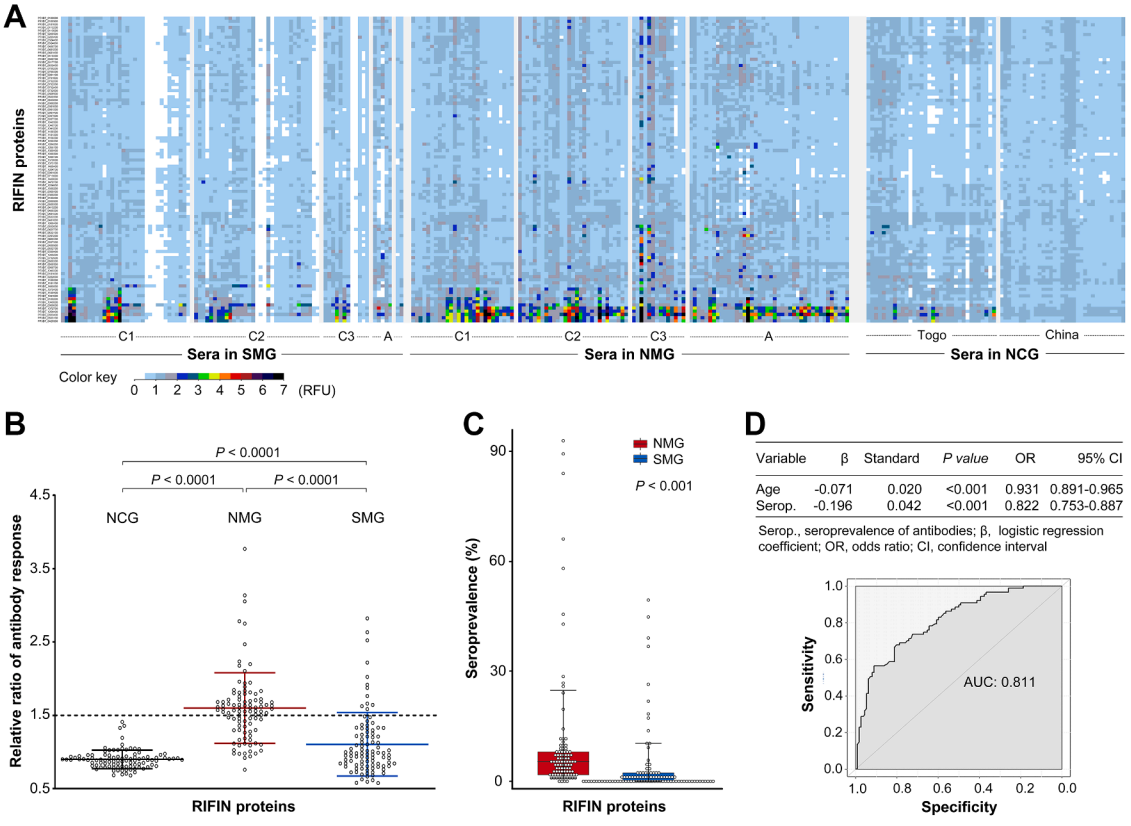

Fig. 1: Anti-RIFIN antibody levels correlate with a reduced risk of severe malaria. (**A**) Protein microarray analysis revealed distinct antibody reactivity patterns against 97 A-RIFINs in severe (SMG, n = 87) and nonsevere (NMG, n = 112) malaria cases compared with those in uninfected controls (NCG, n = 67). The dot plots represent different reactivity patterns of the antibody signal intensity to each RIFIN protein. Positive responses were defined as a signal intensity > 2 SD above the control means. C1, C2, and C3, children aged 0–5, 6–10 and 11–14 years, respectively; A, adults (> 14 years of age). (**B**) Scatter plots showing significantly higher anti-RIFIN antibody levels in the NMG than in the SMG ($P < 0.0001$, Kruskal–Wallis test). The dotted line represents the threshold above which antisera were considered positive responders to the RIFIN proteins. (**C**) Box plots demonstrating greater seroprevalence in NMG across all age groups (Wilcoxon test, $P < 0.001$). The horizontal solid line in each box plot denotes the overall median. (**D**) ROC analysis revealed that anti-RIFIN antibodies and age were independent factors associated with a reduced risk of severe malaria (AUC = 0.811). SMG: severe malaria group; NMG, nonsevere malaria group; NCG, normal control group; RFU, Relative Fluorescence Unit (the fluorescence intensity from each microarray spot is directly proportional to the amount of antibody bound to immobilized RIFIN antigens).

particularly for high-impact variants—may serve as a clinically informative biomarker for improved clinical outcomes.

Identification of RIFIN immunogens associated with a reduced risk of severe malaria

Downselection from 31 immunoreactive candidates allowed to the identification of five RIFIN variants that had the strongest associations with nonsevere malaria status. These RIFINs include PF3D7_0425900, PF3D7_0732400, PF3D7_0833100, PF3D7_0833400 and PF3D7_0900200, hereafter referred to as RIFIN-28, RIFIN-46, RIFIN-54, RIFIN-55 and RIFIN-56, respectively. These prioritized immunogens fit the logistic regression analyses (Hosmer–Lemeshow, χ^2 test $P = 0.6114$, $P = 0.6645$, $P = 0.7679$, $P = 0.7730$, and $P = 0.876$, respectively). While the area under the ROC curve was used to evaluate overall model discrimination (AUC = 0.785–0.808), the odds ratio better reflected the association of each of the five RIFINs with reduced severe malaria risk (association with age: OR = 0.910–0.939, Wald test (Z-score) $P = 0.004$–0.001; association with seroprevalence: OR = 0.104–0.199, Wald test (Z-score) $P < 0.001$; Fig. 2A). All five RIFINs presented significantly greater antibody prevalence in NMG cases than in SMG cases across all age groups (Fisher's exact test (two-sided) $P < 0.0001$; Fig. 2B), with consistently reduced severe malaria risk observed in children aged 0–5 (P = 0.0001–0.0018), 6–10 (P = 0.0001–0.0043), and 11–14 (P = 0.0029–0.0218) years, whereas RIFIN-46 showed attenuated severe malaria risk in adolescents (11–14 years; Fisher's exact test (two-sided) $P = 0.1302$; Fig. 2C).

Anti-RIFIN responses are distinct from those associated with general malaria exposure

The non-VSA antigen control MSP1$_{-42}$ exhibited comparable seroprevalence rates between the NMG and

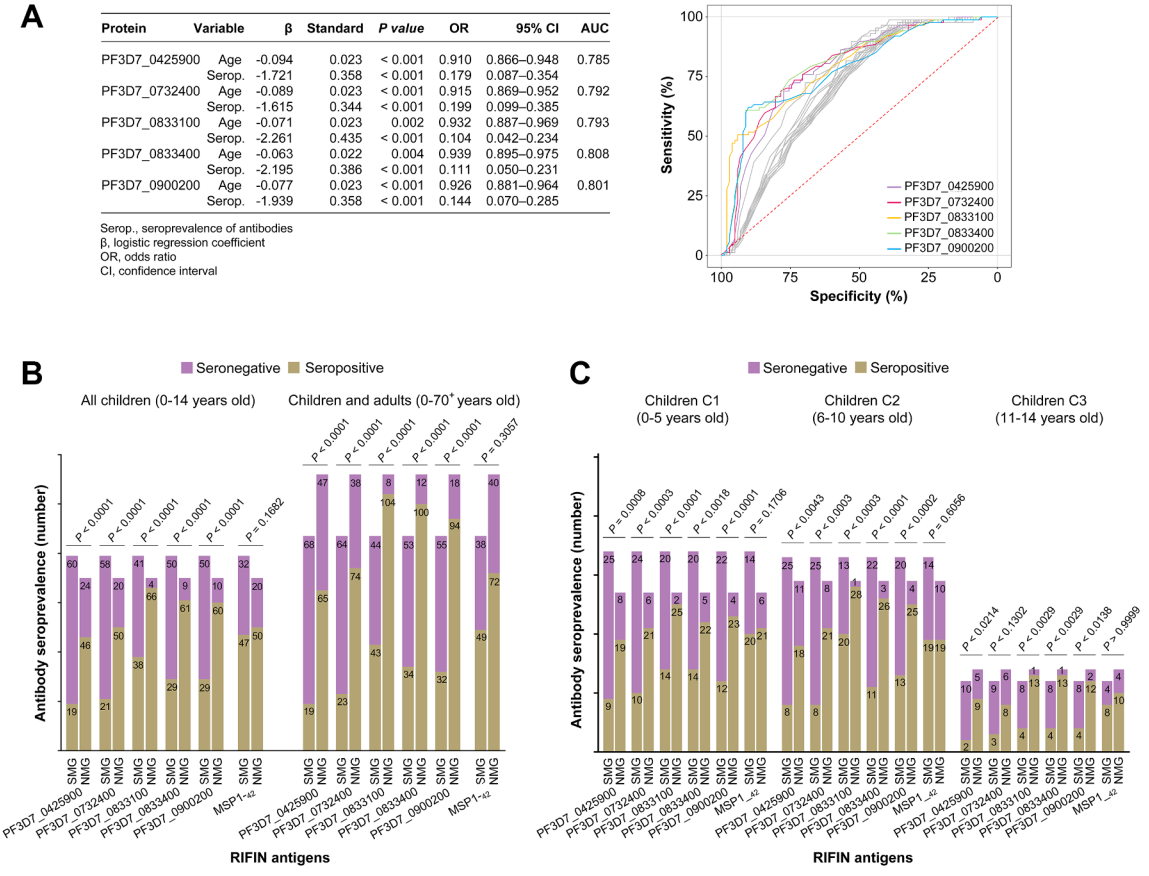

Fig. 2: RIFIN antigens identified as correlates of reduced severe malaria risk. (**A**) The top five RIFIN immunogens (PF3D7_0425900, PF3D7_0732400, PF3D7_0833100, PF3D7_0833400, PF3D7_0900200) significantly associated with milder clinical outcomes (AUC 0.785–0.808; Hosmer–Lemeshow, χ^2 test $P = 0.6114$, $P = 0.6645$, $P = 0.7679$, $P = 0.7730$, $P = 0.876$, respectively; (association with age: OR = 0.910–0.939, Wald test (Z-score) $P = 0.004$–0.001; association with seroprevalence: OR = 0.104–0.199, Wald test (Z-score) $P < 0.001$). (**B**) The top five RIFINs showed significantly greater antibody prevalence in NMG cases than in SMG cases across all age groups (Fisher's exact test (two-sided) $P < 0.0001$). (**C**) Age-stratified analysis confirmed consistent risk reduction in children (0–14 years), unlike the nondiscriminatory response to the MSP1$_{-42}$ control antigen. SMG, severe malaria group; NMG, nonsevere malaria group; NCG, normal control group.

SMG groups across all ages (Fisher's exact test (two-sided) $P = 0.3057$) and among children specifically (Fisher's exact test (two-sided) $P = 0.1682$; Fig. 2B and C), despite stronger immunoreactivity in the NMG than in the SMG (Fig. S3). Additionally, serological analyses that compared anti-RIFIN responses to PfAMA1 and Pf34 control antigens in a subset of NMG/SMG pairs yielded similar results. While RIFIN responses were discordant with those to PfAMA1 and Pf34 antigens, as observed with $MSP1_{-42,}$ and significantly stratified SMG/NMG, the seroprevalence of AMA1 and Pf34 responses was not associated with milder clinical outcomes either (Fisher's exact test (two-sided) $P = 0.0915$ and 0.0958, respectively) (Fig. S4).

RIFIN immunogens exhibit markedly different immunogenicity patterns, which are reflected in their differential immune response capacities. Our data suggest that anti-RIFIN responses are independently associated with severe malaria risk reduction (OR = 0.82, Wald test (Z-score) $P < 0.001$) and show distinct kinetics from non-RIFIN antigens (e.g., no correlation with $MSP1_{-42}$, AMA1, and Pf34). These results underscore a unique and specific profile of RIFIN responses in mediating the clinically reduced risk of severe malaria, independent of general anti-parasite antibody responses.

RIFINs linked to severe malaria risk reduction are LILRB1 ligands with distinct affinities

Building on prior evidence that RIFINs bind LILRB1,[9] we hypothesized that the RIFIN targets associated with severe malaria reduction risk, which are prioritized in this study (RIFIN-28, RIFIN-46, RIFIN-54, RIFIN-55 and RIFIN-56), might similarly engage this inhibitory receptor. Using SPR, we demonstrated binding for four of the RIFIN targets (Fig. 3A), with affinities spanning three orders of magnitude: (1) high affinity: RIFIN-55 (K_D = 3.464 μM) and RIFIN-56 (4.858 μM); (2) moderate affinity: RIFIN-54 (34.05 μM) and RIFIN-28 (42.02 μM); and (3) no detectable binding: RIFIN-46. Notably, RIFIN-55 and RIFIN-56 exhibited affinities comparable to those of physiological LILRB1-MHC class I interactions (2–-7 μM),[53] whereas the positive antigen control RIFIN (PF3D7_1254800) showed superior binding (210.7 nM) (Fig. 3B–G).

Structural mimicry of host MHC-I by RIFIN immunogens

The molecular basis of these interactions was determined via structural models in which LILRB1 complexed with the variable domain of RIFIN-56 (residues 169–321), on the one hand, and with its natural ligand β2-microglobulin, on the another hand, presented key conserved interfaces. Structural modelling revealed that the variable domain of RIFIN-56 adopts a predominantly α-helical fold, with three central helices interconnected by loop regions containing short helical segments (Fig. 4A, Fig. S5A). Molecular modelling revealed two stable binding modes (Model1 and Model2) between RIFIN-56 and the extracellular domain of LILRB1, with Model2 exhibiting greater conservation of interface residues with known LILRB1 complexes (Fig. 4B–C, Fig. S5B–D). Both models showed favourable binding energies (Model1: $E_{BIND} = -111.3 \pm 7.3$ kcal/mol; Model2: –88.5 ± 7.2 kcal/mol) (Fig. S5E–F), although Model2's interface more closely resembled those of the reference complexes LILRB1–PF3D7_1254800 (PDB: 6ZDX) and LILRB1–HLA (PDB: 1P7Q) (Fig. 5A–C).

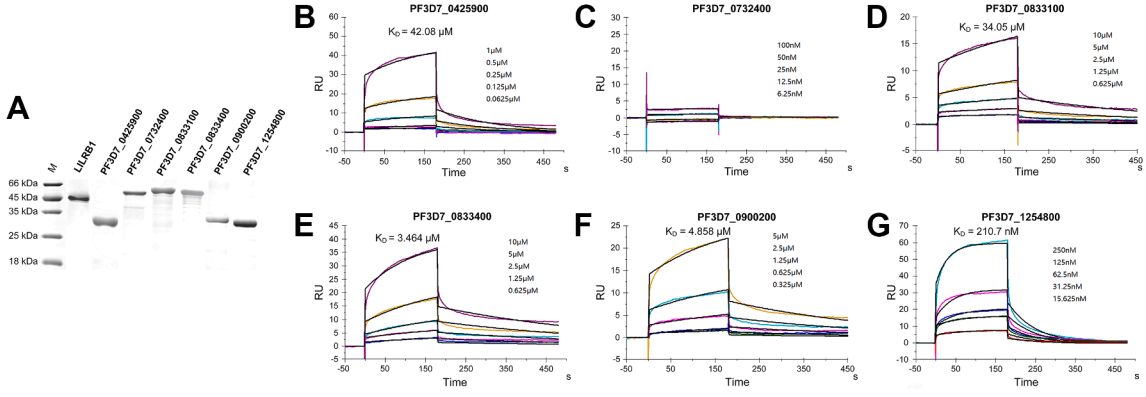

Fig. 3: Validation of RIFINs associated with reduced severe malaria risk as LILRB1 ligands with distinct binding affinities. (**A**) SDS–PAGE confirmed the recombinant expression of the LILRB1 and RIFIN proteins (M: marker). Although the full-length sequences of RIFIN-28, RIFIN-56 and PF3D7_1254800 could not be expressed in a folded form, we were able to produce truncated ectodomains that contained both variable domains. (**B–G**) Surface plasmon resonance (SPR) reveals distinct binding kinetics: RIFIN-28 (1–0.0625 μM), RIFIN-46 (100–6.25 nM), RIFIN-54 (10–0.625 μM), RIFIN-55 (10–0.625 μM), and RIFIN-56 (5–0.325 μM) interact with immobilized LILRB1 (669.2 RU), with PF3D7_1254800 (positive control) showing the strongest binding (250–15.625 nM). All assays used 120 s of association/300 s of dissociation at 30 μl/min. RU, response units.

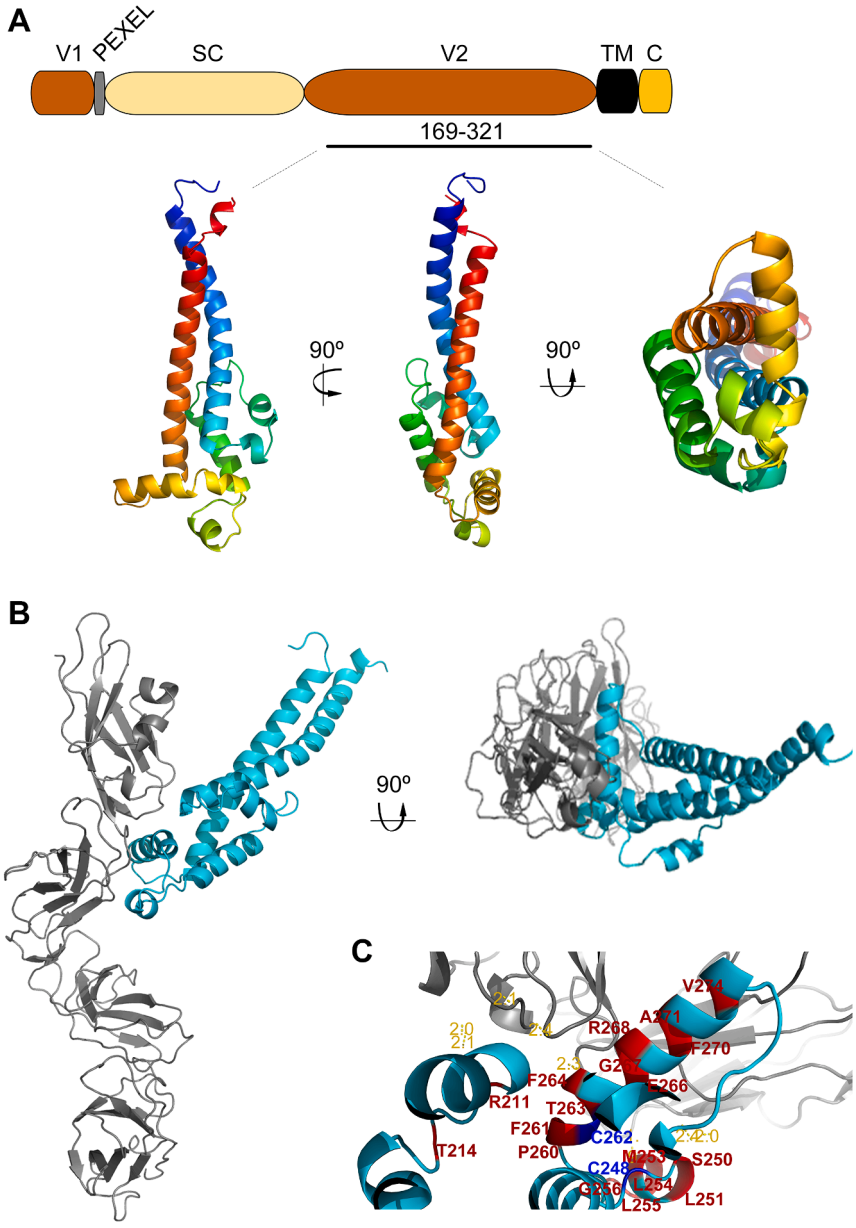

Fig. 4: Molecular architecture of RIFIN–LILRB1 binding. (**A**) Domain architecture of RIFIN-56 (PF3D7_0900200) with a rainbow-colored variable domain structure (blue: N-terminus; red: C-terminus). (**B**) Structure of the RIFIN variable region (cyan) complexed with the LILRB1 ectodomain (gray). (**C**) Detailed interface showing critical interacting residues (red), disulfide-bonded cysteines, and polar contacts (yellow) that mediate binding. Key domains are annotated: V1/V2 (variable), SC (semiconserved), TM (transmembrane), and C (C-terminal conserved). This structural analysis shows the molecular determinants of RIFIN engagement with the inhibitory receptor LILRB1.

Detailed interface analysis demonstrated that RIFIN-56 engages the membrane-distal immunoglobulin-like domains of LILRB1 through a conserved binding core comprising 14 residues flanked by 5–6 variable residues (Fig. 5D–F, Table S7). This structural arrangement reveals remarkable mimicry of the β2-microglobulin interaction mode of MHC-I with LILRB1, despite sequence divergence in surrounding regions (Fig. 5G–I).

Evolutionary balancing act: RIFIN immunogens undergo diversity while retaining conserved features for LILRB1 interactions

Our structural analysis confirmed that despite extensive sequence diversity among RIFIN immunogens, key conserved features mediate their interactions with LILRB1. The binding interface of RIFIN-56 comprises 18 residues (positions 211–274), with 89% of the

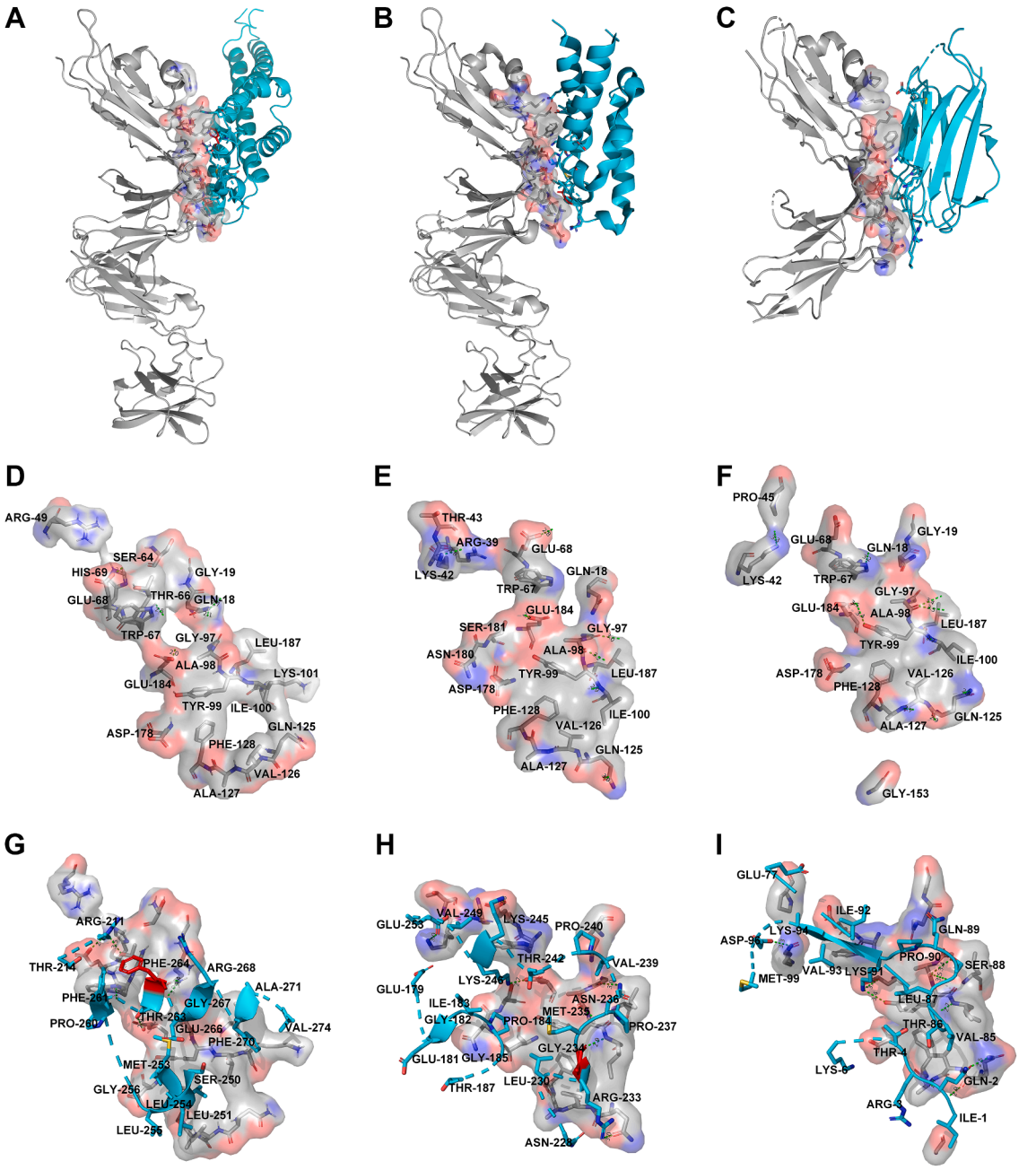

Fig. 5: Comparative structural analysis of the interactions of LILRB1 with the RIFINs and MHC-I. (**A**–**C**) Overview of LILRB1 (gray) bound to (**A**) comptuational RIFIN-56 Model2 (cyan), (**B**) the crystal structure of RIFIN PF3D7_1254800 (6ZDX; cyan), and (**C**) MHC-I β2-microglobulin (1P7Q; cyan). (**D**–**F**) Interface surfaces highlighting binding residues for RIFIN Model2 (**D**), RIFIN 6ZDX (**E**), and β2M (**F**). (**G**–**I**) Detailed interaction networks showing key residues (red), including the functionally validated PHE264 (Model2) and GLY234 (6ZDX) residues. This comparison confirmed convergent binding strategies between pathogenic RIFINs and host MHC-I.

contact area formed by loops and short helices between the second and third main helices. This interface centers around two critical disulfide-bonded cysteines (C248 and C262) that structurally anchor the binding region (Fig. 4C, Fig. S5A). The interaction is stabilized by strong hydrogen bonds (1.9–2.4 Å) involving residues Q209 (2.1 Å), R211 (2.0 Å, 2.1 Å), S250 (2.0 Å, 2.4 Å), M253 (1.9 Å), T263 (2.3 Å) and R268 (2.4 Å), suggesting a physiological binding mode.

Sequence analysis revealed remarkable variability in LILRB1-contacting residues across the RIFIN immunogens (Fig. S6, Fig. 6A), with only two moderately

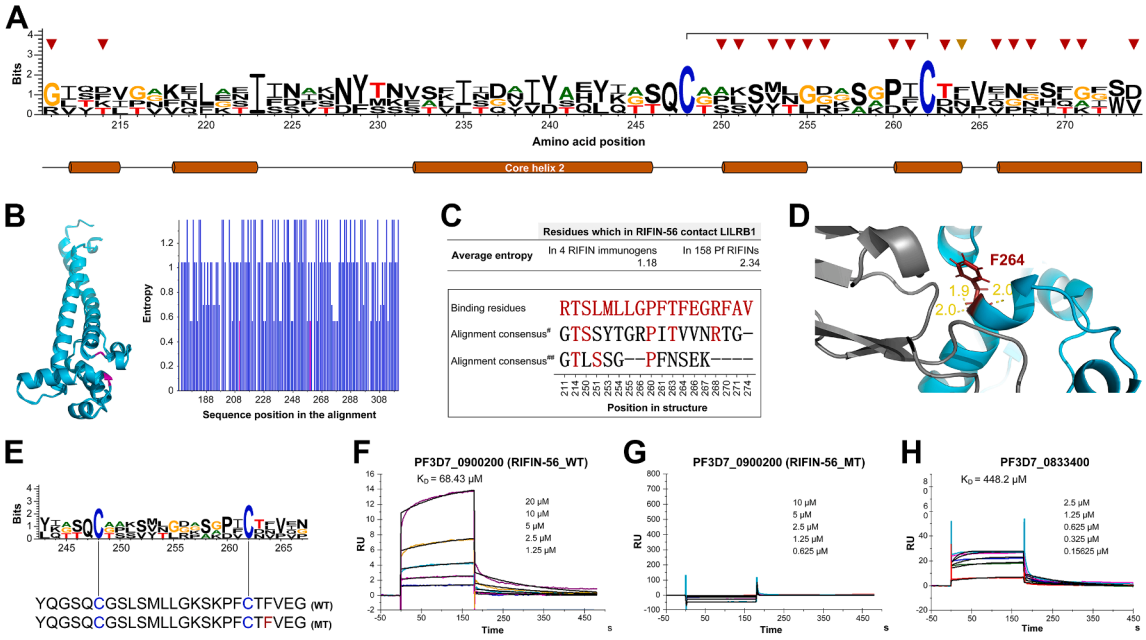

Fig. 6: Conserved structural motifs mediate RIFIN–LILRB1 binding. (**A**) Sequence logo of LILRB1-contacting residues (211–274 of RIFIN-56) highlights conserved features: binding residues (red triangles), critical F264 (gold triangle), and a disulfide bond (bracket). (**B**) Structural map showing position-specific entropy (blue lines) with conserved residues (magenta; entropy = 0.56). (**C**) Comparative entropy analysis revealed greater conservation of binding residues across four newly identified RIFIN immunogens than 158 Pf3D7 RIFINs (dashed lines: no consensus). (**D**) Close-up image of the RIFIN-56–LILRB1 interface showing F264's polar contacts. (**E**) Mutant design (RIFIN-56_MT) targeting this interface. (**F–H**) SPR confirmed that the binding of the F264A mutant (20–156 nM) to LILRB1 was abolished compared with that of the wild-type and positive controls (PF3D7_1254800). RU: response units. # Alignment consensus for the residues in RIFIN-56 that contact LILRB1 in the 4 RIFIN immunogens identified in this study. ## Alignment consensus for the residues in RIFIN-56 that contact LILRB1 in 158 RIFINs homologous of Pf 3D7.

conserved positions (R211 and P260, entropy = 0.56) among the four identified binding RIFINs (Fig. 6B). This diversity becomes even more pronounced when 158 RIFIN homologues, where no conserved contact residues were identified (entropy > 1; Fig. S7), were examined. However, the disulfide-bonded cysteine pair remains invariant, forming a structural scaffold that maintains binding competence despite surrounding sequence variation (Fig. S6). Compared with those in the broader RIFIN family, the contact residues in the four immunogens presented greater consensus (lower entropy) (Fig. 6C), suggesting evolutionary selection for functional binding modes within RIFIN variants.

Structural constraints maintain conserved LILRB1-binding motifs in RIFIN immunogens

We investigated how sequence diversification impacts receptor binding, by focusing on a critical phenylalanine residue (F264) within the LILRB1-binding interface of RIFIN-56. This residue forms three key hydrogen bonds (1.9, 2.0, and 2.0 Å) with LILRB1 while being proximal to the structurally essential disulfide bond (Fig. 6D). We engineered a truncated mutant (residues 243–267) containing the core binding motif, including both conserved cysteines, and introduced an F264A substitution (RIFIN-56_F264A) to test the functional consequences of disrupting this polar network (Fig. 6E).

SPR analysis revealed complete loss of detectable LILRB1 binding to RIFIN-56_F264A, whereas the wild-type peptides (RIFIN-56_WT and positive control PF3D7_1254800) maintained strong interactions (Fig. 6F–H). This result occurred despite the preserved overall structure, demonstrating that F264's specific chemical properties—rather than global folding—are essential for maintaining the hydrogen-bonding pattern required for LILRB1 engagement.

Our work systematically identifies a subset of RIFINs linked to reduced severe malaria risk and reveals how structural and chemical constraints limit the diversification of key interfacial residues in these RIFINs, preserving their ability to mimic host ligands despite extensive sequence variation elsewhere.

Discussion

Plasmodium falciparum has evolved sophisticated strategies to balance immune evasion with host interaction through VSAs.[2,9] RIFINs undergo antigenic variation, and anti-RIFIN antibodies are linked to clinical malaria

outcomes.[3,11] Since then, the spectrum of RIFIN implications in clinical immunity and disease progression has been questioned. While it is not surprising that surface-exposed antigens provoke immune responses, the structural and functional basis by which RIFINs are associated with clinical outcomes has remained unclear.

This study bridges critical gaps in the understanding of how RIFINs elicit antibodies associated with a reduced risk of severe malaria and maintain receptor-binding capacity while evading immune detection.

RIFIN response correlated with milder clinical outcomes

While cerebral malaria, organ failure, or severe malarial anaemia was not observed in the SMG cohort, the WHO-defined severe manifestations of malaria cases share common pathophysiological pathways of endothelial dysfunction and metabolic acidosis. Our SMG cohort was clinically heterogenous between different severe manifestations; however, the primary objective of this study was to identify RIFIN targets associated with a reduced risk of severe malaria as a composite WHO endpoint. This approach of severe phenotype grouping was strategically chosen because (1) our power calculations required grouping to detect significant associations given sample size constraints; (2) the shared feature of all severe cases — high parasite biomass and systemic inflammation — suggests common immunological pressure points that RIFINs may exploit; (3) our primary endpoint — RIFIN immunogenicity — showed consistent patterns of anti-RIFIN responses across all severe phenotypes ($P = 0.32$ for heterogeneity test); and (4) this approach aligns with recent multicentre severe malaria studies that demonstrate shared host–response mechanisms across severity spectra.[54]

Our systematic analysis of humoral responses against all IE-surface RIFINs revealed significantly higher anti-RIFIN antibody levels in NMG subjects than in SMG subjects ($P < 0.001$), particularly in children (0–14 years). These findings align with epidemiological studies from Mali, Gabon, and Uganda showing that anti-RIFIN antibodies are correlated with milder clinical outcomes of malaria.[11,15–17] While these studies link anti-RIFIN antibodies to improved clinical outcomes, they do not establish causal protection, and responses may also reflect cumulative exposure. We identified 31 RIFIN variants, including 17 newly reported immunogens (PF3D7_0200500, PF3D7_0222600, PF3D7_0324400, PF3D7_0600500, PF3D7_0600700, PF3D7_0632100, PF3D7_0701800, PF3D7_0732200, PF3D7_0832500, PF3D7_0900600, PF3D7_0901400, PF3D7_0937500, PF3D7_1101300, PF3D7_1254400, PF3D7_1255100, PF3D7_1300700, and PF3D7_1373100), alongside 14 previously recognized targets.[3,10,14–16,55–57] The top five immunogens (RIFIN-28, RIFIN-46, RIFIN-54, RIFIN-55, and RIFIN-56) were significantly strongly associated with reduced a risk of severe malaria in Togolese children, mirroring findings from Liberia, Gambia, and Kenya.[3,15,16] Unlike the vaccine candidates $MSP1_{-42}$, AMA1, and P34,[30] which showed comparable seroprevalence between the SMG and NMG groups, RIFIN-specific responses clearly demonstrated clinical stratification. Our data highlighted a unique and independent association of RIFIN immunogens with severe malaria risk reduction (OR = 0.82, Wald test (Z-score) $P < 0.001$), showed distinct kinetics from non-RIFIN antigens (e.g., no correlation with $MSP1_{-42}$, AMA1, and Pf34), and aligned with prior evidence that RIFIN–LILRB1 interactions modulate immune evasion.[10] However, future studies should track antibody dynamics to establish temporal relationships and test functional mechanisms (e.g., LILRB1 blockade assays).

The associations between anti-RIFIN seroprevalence and reduced malaria severity across diverse demographic groups position RIFIN immunogens as (1) promising vaccine targets for inducing clinical immunity and (2) potential biomarkers for stratifying severe malaria risk in endemic populations. Thus, RIFINs might have translational value as both therapeutic targets and prognostic tools in malaria control strategies.

Molecular mimicry and immune evasion: a conserved RIFIN–LILRB1 structural blueprint

The molecular mimicry we found between the RIFINs associated with severe malaria reduction risk and host MHC-I aligned with that reported in other RIFINs by Harrison et al.,[10] and represents a master class in pathogen deception. In this study, we demonstrate that the RIFIN immunogens (RIFIN-56, RIFIN-54, RIFIN-55, and RIFIN-56) bind LILRB1, notably with affinities for RIFIN-55 and RIFIN-56 (3.464 and 4.858 μM, respectively), comparable to physiological LILRB1–β2M interactions (2–7 μM)[53] or to previously reported pathogenic LILRB1–RIFINs (PF3D7_1254800, PF3D7_0223100, and PF3D7_0100400) interactions.[9,10] While these structural models reflected in key conserved interfaces may explain the differential binding affinities observed experimentally, they revealed remarkable convergence between the RIFIN– and MHC-I–binding modes, with 14 conserved core residues maintaining the interaction interface despite extensive peripheral sequence variation. This evolutionary finding via a disulfide-anchored "molecular velcro" system paralleled bacterial immune evasion proteins such as *Staphylococcus aureus* SSL7.[12] The LILRB1-binding domain features a disulfide-stabilized loop (Cys–Cys 1.9–2.4 Å distance matching human CD2/CD58 interfaces) that positions key hydrogen bond donors/acceptors as a structural linchpin, mirroring recently reported RIFIN architectures and resembling PfEMP1–EPCR interactions.[10,58] The shared binding geometry between RIFINs and physiological MHC-I ligands suggests an evolutionary strategy that exploits the natural

recognition machinery of LILRB1—molecular mimicry of host receptors—while incorporating strain-specific variations that may facilitate immune evasion. This may explain how RIFINs maintain receptor engagement amid antigenic variation through conserved structural frameworks supporting diverse surface chemistries.

Constraints on immune evasion strategies

Our findings align with those of previous studies that reported the elegant evolutionary and structural ingenuity of RIFINs.[10,18] While maintaining overall binding functionality with LILRB1 through a conserved disulfide-stabilized architecture, sequence diversification in contact residues enables immune nonrecognition through antigenic variation. However, mutagenesis studies revealed strict limitations in the diversification of the RIFINs prioritized in this study. The F264A mutation in the RIFIN-56 binding motif abolished LILRB1 recognition despite preserving the overall structure, demonstrating how chemical constraints maintain interaction capacity.[10] Sequence analysis revealed that while surface residues vary widely, all the LILRB1-binding RIFINs retain (1) the conserved disulfide-bonded loop and (2) residues with compatible hydrogen-bonding potential at critical positions. For example, RIFIN-28, RIFIN-54, and RIFIN-55 utilize Leu238, Leu260, and Asn248, respectively, at positions equivalent to RIFIN-56's Phe264, maintaining interaction chemistry through different residues. This "conserved architecture, diverse chemistry" paradigm represents an elegant evolutionary solution to balance immune evasion with receptor engagement.

While structural models align with prior crystallographic evidence demonstrating RIFIN mimicry of MHC-I,[10,18] this study uniquely identifies a RIFIN subset linked to clinical outcomes and reveals how a conserved structural motif enables receptor engagement across this diverse subset, providing a mechanistic basis for their role in immune evasion and clinical immunity.

The novelty of our approach lies in integrating high-throughput immunoproteomics with structural biology and biophysical validation to bridge molecular mechanisms and clinical outcomes. This study not only pinpointed the antibody responses of specific RIFIN variants correlated with milder clinical outcomes but also demonstrated functional interactions of the RIFIN variants with LILRB1, elucidated the structural mimicry of MHC-I, and identified a disulfide-stabilized binding core that is conserved across the variants. This motif represents a vulnerability that can be exploited for rational intervention—guiding the design of vaccines or monoclonal antibodies that disrupt immune evasion across diverse RIFIN strains.

While our study focused on the structural determinants of RIFIN–LILRB1 binding, prior work has established that anti-RIFIN antibodies can block this interaction.[9,10] Future studies should define the specific antibody subtypes (e.g., IgG1 vs. IgG3) and epitopes responsible for neutralization, which could guide monoclonal antibody development.

Therapeutic implications

The conserved molecular architecture we identified presents both opportunities and challenges for malaria intervention strategies. With over half a million malaria deaths annually—primarily African children under five[1]—the need for innovative solutions targeting severe malaria has never been greater. The identification of the "conserved core, diverse surface" paradigm in RIFINs associated with clinical malaria outcomes echoes successful strategies against other pathogens; much like the conserved CD4-binding site of the HIV envelope, which enables broadly neutralizing antibodies,[59] RIFIN disulfide-stabilized loops anchor next-generation immunogens.

Three transformative opportunities emerge. First, structure-guided vaccines targeting the conserved cysteine loop could elicit antibodies that broadly disrupt LILRB1 interactions, akin to recent advances in respiratory syncytial virus vaccines.[60] Second, small molecules mimicking key hydrogen-bond networks (e.g., the 1.9–2.4 Å interactions we identified) might block receptor engagement—a strategy proving effective against SARS-CoV-2.[5] Third, engineered monoclonal antibodies could combine the broad recognition capacity of LILRB1 with Fc-mediated effector functions, following the model of malaria-neutralizing CIS43.[61]

As drug resistance spreads,[62] targeting host–pathogen interfaces such as RIFIN–LILRB1 offers a promising evolutionary constraint against parasite escape. Combining RIFIN-targeting approaches with current MSP-based vaccines may lead to synergistic improvements in clinical malaria outcomes.

Study limitations and future directions

Our study has several limitations, which frame clear avenues for future translational research implications. First, although our study did not replicate blocking assays, earlier studies confirmed that anti-RIFIN antibodies can inhibit LILRB1 engagement. Future work should directly test whether qualitative differences in antibody function distinguish nonsevere from severe cases—such as the ability to block LILRB1 binding—and correlate with clinical outcomes through longitudinal studies to confirm protective efficacy. Second, while our composite severe malaria grouping enabled the detection of RIFIN associations, which is consistent with WHO intervention targets, future studies with larger cohorts should examine whether specific RIFIN variants show preferential associations with distinct severe malaria syndromes (e.g., cerebral malaria vs. severe anaemia). This stratification may reveal additional pathophysiological nuances in RIFIN-mediated

immune evasion. Our study also confirmed a conserved structural motif—centered on disulfide-bonded cysteines—that appears fundamental to LILRB1 engagement in the 3D7 reference strain; however, its persistence across global isolates requires further experimental verification to confirm its universal therapeutic potential. Finally, we acknowledge that both age and anti-RIFIN antibody levels are influenced by prior infections; however, precise data on the frequency of prior malaria infections for each participant are lacking, as this retrospective clinical information was not systematically collected in our cohort. We adjusted for known proxies of exposure (e.g., age and geographic origin) in our multivariate models to mitigate this confounding effect.

Moreover, although not all RIFINs have been experimentally tested to date, the conserved disulfide motif suggests that the binding potential of LILRB1 may be widespread, albeit with varying affinities or functional outcomes. Future work should systematically profile LILRB1 binding across global RIFIN diversity to address this issue clearly.

In conclusion, our work identified a subset of RIFINs linked to reduced severe malaria risk and confirmed a conserved structural motif through which they engage the inhibitory receptor LILRB1, despite extreme sequence diversity. This evolutionary and structural ingenuity of RIFINs underscore their ability to maintain receptor-binding function through a conserved architectural element while varying surrounding sequences to evade immune detection. Like PfEMP1, RIFINs represent a family of variant antigens capable of eliciting antibodies associated with severe malaria risk reduction. However, their structurally conserved immune evasion motif—and their engagement in the immunosuppressive LILRB1 pathway—may offer unique advantages for interventions aimed at counteracting parasite-mediated immunosuppression while promoting humoral immunity. These findings directly inform translational strategies for the development of structure-guided vaccines or monoclonal antibodies to disrupt LILRB1 interactions. By bridging molecular mechanisms with epidemiological evidence, our work redefines RIFINs as actionable targets, urging further translational validation in diverse endemic settings to accelerate their path from bench to bedside.

Contributors

Conceptualization: K.K. and J-H.C. Methodology: K.K., H-M.S., and J-H.C. Investigation: K.K. Visualization: K.K. and J-H.C. Formal analysis: K.K., S-J.X., and J.L. Validation: K.K., J-H.C, X–N.Z., and K.W.D. Resources: S-B.C., B.X., and Y.W. Data curation: K.K. and H-M.S. Funding acquisition: J-H.C. and Y.W. Project administration: K.K., J-H.C., and X-N.Z. Supervision: J-H.C. and X-N.Z. Writing—original draft: K.K. Writing—review and editing: K.K., J-H.C., and K.W.D. All the authors have read and approved the final version of the manuscript, K.K. and J-H.C. have accessed and verified the underlying data.

Data sharing statement

The data supporting the findings of this study and the protocols are included in the article and supplementary data. Further inquiries can be directed to the corresponding authors.

Declaration of interests

All the other authors declare that they have no competing interests.

Acknowledgements

The authors thank Ms. Zhi-Shan Sun (former Master candidate at the School of Global Health, Shanghai Jiao Tong University School of Medicine) for assisting in performing the regression analyses and Dr. Qun-Feng Wu (Eosvision medtech Co., Ltd.) for completing the structural model analyses.

Appendix A. Supplementary data

Supplementary data related to this article can be found at https://doi.org/10.1016/j.ebiom.2025.106041.

References

1 World Health Organization, (WHO). World Malaria Report 2023. https://www.who.int/teams/global-malaria-programme/reports/world-malaria-report-2023. Accessed November 30, 2023.
2 Kyes SA, Rowe JA, Kriek N, Newbold CI. Rifins: a second family of clonally variant proteins expressed on the surface of red cells infected with *Plasmodium falciparum*. *Proc Natl Acad Sci U S A*. 1999;96:9333–9338.
3 Fernandez V, Hommel M, Chen Q, Hagblom P, Wahlgren M. Small, clonally variant antigens expressed on the surface of the *Plasmodium falciparum*-infected erythrocyte are encoded by the rif gene family and are the target of human immune responses. *J Exp Med*. 1999;190:1393–1404.
4 Lawton JG, Zhou AE, Stucke EM, et al. Diamonds in the rif: alignment-free comparative genomics analysis reveals strain-transcendent *Plasmodium falciparum* antigens amidst extensive genetic diversity. *Infect Genet Evol*. 2025;129:105725.
5 Joannin N, Abhiman S, Sonnhammer EL, Wahlgren M. Sub-grouping and sub-functionalization of the RIFIN multi-copy protein family. *BMC Genomics*. 2008;9:19.
6 Petter M, Haeggstrom M, Khattab A, Fernandez V, Klinkert MQ, Wahlgren M. Variant proteins of the *Plasmodium falciparum* RIFIN family show distinct subcellular localization and developmental expression patterns. *Mol Biochem Parasitol*. 2007;156:51–61.
7 Bachmann A, Petter M, Tilly AK, et al. Temporal expression and localization patterns of variant surface antigens in clinical *Plasmodium falciparum* isolates during erythrocyte schizogony. *PLoS One*. 2012;7:e49540.
8 Goel S, Palmkvist M, Moll K, et al. RIFINs are adhesins implicated in severe *Plasmodium falciparum* malaria. *Nat Med*. 2015;21:314–317.
9 Saito F, Hirayasu K, Satoh T, et al. Immune evasion of *Plasmodium falciparum* by RIFIN via inhibitory receptors. *Nature*. 2017;552:101–105.
10 Harrison TE, Morch AM, Felce JH, et al. Structural basis for RIFIN-mediated activation of LILRB1 in malaria. *Nature*. 2020;587:309–312.
11 Abdel-Latif MS, Dietz K, Issifou S, Kremsner PG, Klinkert MQ. Antibodies to *Plasmodium falciparum* rifin proteins are associated with rapid parasite clearance and asymptomatic infections. *Infect Immun*. 2003;71:6229–6233.
12 Abdel-Latif MS, Khattab A, Lindenthal C, Kremsner PG, Klinkert MQ. Recognition of variant Rifin antigens by human antibodies induced during natural *Plasmodium falciparum* infections. *Infect Immun*. 2002;70:7013–7021.
13 Sun ZS, Yin JX, Zhao HQ, et al. Conserved multiepitopes in STEVORs enable rational design of a fusion antigen vaccine construct with broad immunogenicity. *Emerg Microbes Infec*. 2025;14:2552783.
14 Tan J, Pieper K, Piccoli L, et al. A LAIR1 insertion generates broadly reactive antibodies against malaria variant antigens. *Nature*. 2016;529:105–109.
15 Zhou AE, Berry AA, Bailey JA, et al. Antibodies to peptides in semiconserved domains of RIFINs and STEVORs correlate with malaria exposure. *mSphere*. 2019;4:e00097.

16 Travassos MA, Niangaly A, Bailey JA, et al. Children with cerebral malaria or severe malarial anaemia lack immunity to distinct variant surface antigen subsets. *Sci Rep*. 2018;8:6281.
17 Kanoi BN, Nagaoka H, White MT, et al. Global repertoire of human antibodies against *Plasmodium falciparum* RIFINs, SURFINs, and STEVORs in a malaria exposed population. *Front Immunol*. 2020;11:893.
18 Chen Y, Xu K, Piccoli L, et al. Structural basis of malaria RIFIN binding by LILRB1-containing antibodies. *Nature*. 2021;592:639–643.
19 Chen JH, Jung JW, Wang Y, et al. Immunoproteomics profiling of blood stage *Plasmodium vivax* infection by high-throughput screening assays. *J Proteome Res*. 2010;9:6479–6489.
20 Kassegne K, Abe EM, Chen JH, Zhou XN. Immunomic approaches for antigen discovery of human parasites. *Expert Rev Proteomics*. 2016;13:1091–1101.
21 Fan YT, Wang Y, Ju C, et al. Systematic analysis of natural antibody responses to P. falciparum merozoite antigens by protein arrays. *J Proteomics*. 2013;78:148–158.
22 Kassegne K, Fei SW, Ananou K, et al. A molecular investigation of malaria infections from high-transmission areas of Southern Togo reveals different species of *plasmodium* parasites. *Front Microbiol*. 2021;12:732923.
23 Kassegne K, Komi Koukoura K, Shen HM, et al. Genome-wide analysis of the malaria parasite *Plasmodium falciparum* isolates from Togo reveals selective signals in immune selection-related antigen genes. *Front Immunol*. 2020;11:552698.
24 Xu Q, Liu S, Kassegne K, et al. Genetic diversity and immunogenicity of the merozoite surface protein 1 C-terminal 19-kDa fragment of *Plasmodium ovale* imported from Africa into China. *Parasit Vectors*. 2021;14:583.
25 Shen FH, Ong JJY, Sun YF, et al. A chimeric *Plasmodium vivax* Merozoite surface protein antibody recognizes and blocks erythrocytic *P. cynomolgi* berok merozoites in vitro. *Infect Immun*. 2021;89:e00645.
26 Fu H, Lu J, Zhang X, et al. Identification of the recombinant *Plasmodium vivax* surface-related antigen as a possible immune evasion factor against human splenic fibroblasts by targeting ITGB1. *Front Cell Dev Biol*. 2021;9:764109.
27 Bohme U, Otto TD, Sanders M, Newbold CI, Berriman M. Progression of the canonical reference malaria parasite genome from 2002-2019. *Wellcome Open Res*. 2019;4:58.
28 Berrow NS, Alderton D, Owens RJ. The precise engineering of expression vectors using high-throughput In-Fusion PCR cloning. *Methods Mol Biol*. 2009;498:75–90.
29 Kassegne K, Zhang T, Chen SB, et al. Study roadmap for high-throughput development of easy to use and affordable biomarkers as diagnostics for tropical diseases: a focus on malaria and schistosomiasis. *Infect Dis Poverty*. 2017;6:130.
30 Zhou X, Zhang Q, Chen JH, Dai JF, Kassegne K. Revisiting the antigen markers of vector-borne parasitic diseases identified by immunomics: identification and application to disease control. *Expert Rev Proteomics*. 2024;21:205–216.
31 Segireddy RR, Belda H, Yang ASP, et al. A screen for sporozoite surface protein binding to human hepatocyte surface receptors identifies novel host-pathogen interactions. *Malaria J*. 2024;23:151.
32 WHO. Severe malaria. *Trop Med Int Health*. 2014;19(Suppl 1):7–131.
33 Mirdita M, Schutze K, Moriwaki Y, Heo L, Ovchinnikov S, Steinegger M. ColabFold: making protein folding accessible to all. *Nat Methods*. 2022;19:679–682.
34 Steinegger M, Soding J. MMseqs2 enables sensitive protein sequence searching for the analysis of massive data sets. *Nat Biotechnol*. 2017;35:1026–1028.
35 Jumper J, Evans R, Pritzel A, et al. Highly accurate protein structure prediction with AlphaFold. *Nature*. 2021;596:583–589.
36 Baek M, DiMaio F, Anishchenko I, et al. Accurate prediction of protein structures and interactions using a three-track neural network. *Science*. 2021;373:871–876.
37 Kozakov D, Hall DR, Xia B, et al. The ClusPro web server for protein-protein docking. *Nat Protoc*. 2017;12:255–278.
38 Case DA, Betz RM, Cerutti DS, et al. *AMBER 2016*. San Francisco: University of California; 2016.
39 Hess B, Bekker H, Berendsen HJC, Fraaije JGEM. LINCS: a linear constraint solver for molecular simulations. *J Comput Chem*. 1998;18:1463–1472.
40 Aqvist J. Ion water interaction potentials derived from free-energy perturbation simulations. *J Phys Chem*. 1990;94:8021–8024.
41 Jorgensen WL, Chandrasekhar J, Madura JD. Comparison of simple potential functions for simulating liquid water. *J Phys Chem*. 1983;79:926–935.
42 Gordon JC, Myers JB, Folta T, Shoja V, Heath LS, Onufriev A. H++: a server for estimating pKas and adding missing hydrogens to macromolecules. *Nucleic Acids Res*. 2005;33:W368–W371.
43 Maier JA, Martinez C, Kasavajhala K, Wickstrom L, Hauser KE, Simmerling C. ff14SB: improving the accuracy of protein side chain and backbone parameters from ff99SB. *J Chem Theory Comput*. 2015;11:3696–3713.
44 Hoover WG. Canonical dynamics - equilibrium phase-space distributions. *Phys Rev*. 1985;31:1695–1697.
45 Zhang Y, Feller SE, Brooks BR, Pastor RW. Computer simulation of liquid/liquid interfaces. I. Theory and application to octane/water. *J Phys Chem*. 1995;103:10252–10266.
46 Toukmaji A, Sagui C, Board J, Darden T. Efficient particle-mesh Ewald based approach to fixed and induced dipolar interactions. *J Phys Chem*. 2000;113:10913–10927.
47 Kumari R, Kumar R, Open Source Drug Discovery C, Lynn A. g_mmpbsa–a GROMACS tool for high-throughput MM-PBSA calculations. *J Chem Inf Model*. 2014;54:1951–1962.
48 Srinivasan J, Miller J, Kollman PA, Case DA. Continuum solvent studies of the stability of RNA hairpin loops and helices. *J Biomol Struct Dyn*. 1998;16:671–682.
49 Wang E, Sun H, Wang J, et al. End-point binding free energy calculation with MM/PBSA and MM/GBSA: strategies and applications in drug design. *Chem Rev*. 2019;119:9478–9508.
50 Kollman PA, Massova I, Reyes C, et al. Calculating structures and free energies of complex molecules: combining molecular mechanics and continuum models. *Acc Chem Res*. 2000;33:889–897.
51 Edgar RC. MUSCLE: multiple sequence alignment with high accuracy and high throughput. *Nucleic Acids Res*. 2004;32:1792–1797.
52 Crooks GE, Hon G, Chandonia JM, Brenner SE. WebLogo: a sequence logo generator. *Genome Res*. 2004;14:1188–1190.
53 Wang Q, Song H, Cheng H, et al. Structures of the four Ig-like domain LILRB2 and the four-domain LILRB1 and HLA-G1 complex. *Cell Mol Immunol*. 2020;17:966–975.
54 Seydel KB, Kampondeni SD, Valim C, et al. Brain swelling and death in children with cerebral malaria. *N Engl J Med*. 2015;372:1126–1137.
55 Arora G, Hart GT, Manzella-Lapeira J, et al. NK cells inhibit *Plasmodium falciparum* growth in red blood cells via antibody-dependent cellular cytotoxicity. *Elife*. 2018;7:e36806.
56 Nilsson Bark SK, Ahmad R, Dantzler K, et al. Quantitative proteomic profiling reveals novel *Plasmodium falciparum* surface antigens and possible vaccine candidates. *Mol Cell Proteomics*. 2018;17:43–60.
57 Kanoi BN, Takashima E, Morita M, et al. Antibody profiles to wheat germ cell-free system synthesized *Plasmodium falciparum* proteins correlate with protection from symptomatic malaria in Uganda. *Vaccine*. 2017;35:873–881.
58 Lau CK, Turner L, Jespersen JS, et al. Structural conservation despite huge sequence diversity allows EPCR binding by the PfEMP1 family implicated in severe childhood malaria. *Cell Host Microbe*. 2015;17:118–129.
59 Bachmann A, Scholz JA, Janssen M, et al. A comparative study of the localization and membrane topology of members of the RIFIN, STEVOR and PfMC-2TM protein families in *Plasmodium falciparum*-infected erythrocytes. *Malar J*. 2015;14:274.
60 Bultrini E, Brick K, Mukherjee S, et al. Revisiting the *Plasmodium falciparum* RIFIN family: from comparative genomics to 3D-model prediction. *BMC Genomics*. 2009;10:445.
61 Joannin N, Kallberg Y, Wahlgren M, Persson B. RSpred, a set of hidden Markov models to detect and classify the RIFIN and STEVOR proteins of *Plasmodium falciparum*. *BMC Genomics*. 2011;12:119.
62 Khattab A, Klinkert MQ. Maurer's clefts-restricted localization, orientation and export of a *Plasmodium falciparum* RIFIN. *Traffic*. 2006;7:1654–1665.